# High-precision camera distortion measurements with a "calibration harp"

Z. Tang,[1,*] R. Grompone von Gioi,[2] P. Monasse,[3] and J.M. Morel[2]

[1]*ECE, University of Minnesota, Minneapolis, USA*

[2]*CMLA, ENS Cachan, France*

[3]*IMAGINE, Ecole des Ponts ParisTech, France*

[*]*Corresponding author: tangfrch@gmail.com*

 This paper addresses the high precision measurement of the distortion of a digital camera from photographs. Traditionally, this distortion is measured from photographs of a flat pattern which contains aligned elements. Nevertheless, it is nearly impossible to fabricate a very flat pattern and to validate its flatness. This fact limits the attainable measurable precisions. In contrast, it is much easier to obtain physically very precise straight lines by tightly stretching good quality strings on a frame. Taking literally "plumb-line methods", we built a "calibration harp" instead of the classic flat patterns to obtain a high precision measurement tool, demonstrably reaching 2/100 pixel precisions. The harp is complemented with the algorithms computing automatically from harp photographs three different and complementary lens distortion measurements. The precision of the method is evaluated on images corrected by state-of-the-art distortion correction algorithms, and by popular software. Three applications are shown: first an objective and reliable measurement of the result of any distortion correction. Second, the harp permits to control state-of-the art global camera calibration algorithms: It permits to select the right distortion model, thus avoiding internal compensation errors inherent to these methods. Third, the method replaces manual procedures in other distortion correction methods and increases their reliability and precision. © 2012 Optical Society of America

Our lens distortion measurement algorithm can be tested on the online demo version available at `http://bit.ly/lens-distortion`.

## 1. Introduction

The precision of 3D stereovision applications is intimately related to the precision of the camera calibration, and especially of the camera distortion correction. An imprecise distortion model produces residual distortion that will be directly back-projected to the reconstructed 3D scene. Such imprecision can be a serious hindrance in remote sensing applications such as the early warnings of geology disasters, or in the construction of topographic maps from stereographic pairs of aerial photographs. The fast growing resolution of digital cameras and of their optical quality is transforming them into (potential) high precision measurement tools. Thus, it becomes important to measure the calibration precision with ever higher precision.

A first step toward high-precision distortion corrections is to perform precise distortion measurements. This basic tool can then be used to evaluate the precision of a correction method, or can become part of the correction method itself.

Camera and lens distortion measurement methods usually require a flat pattern containing aligned elements. The pattern is photographed using the target lens, and the distortion is measured by how much the observed elements deviate from the straight alignment on the pattern. For example, in its classic evaluation method representing well the camera maker practice, DxO-labs'software (`http://www.dxo.com/`) uses a pattern with a grid of aligned dots. Distortion is measured by the positional errors associated with the maximal deviation in a row, see Fig. 1. Similar methods are proposed by the SMIA[1], EBU[2], IE[3], and I3A[4] standards. All of these measurements are manual and require a perfectly flat pattern.

Every lens distortion correction method includes, implicitly, a lens distortion measurement. These methods can be roughly classified into four groups:

- re-projection error minimization methods;

- pattern matching methods;

- enlarged epipolar geometry based methods;

- plumb-line methods.

Re-projection methods usually rely on a planar pattern containing simple geometric shapes. In these methods, the lens distortion is estimated together with the camera internal and external parameters [1–5], by minimizing the re-projection error between the observed control points on the pattern and the re-projected control points simulated by the pattern

---

[1]Standard Mobile Imaging Architecture standard
[2]European Broadcasting Union standard `http://www.ebu.ch/`
[3]Image Engineering standard `http://www.image-engineering.de/`
[4]International Imaging Industry Association standard `http://www.i3a.org/`

Distortion (%) = $\frac{I}{L} \times 100$

Calculation of distortion from an image of the dot chart.
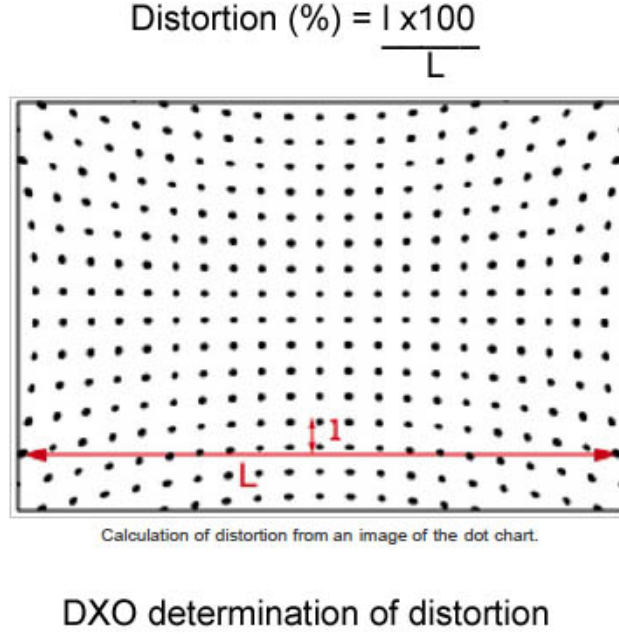
DXO determination of distortion

Fig. 1: DxO lens distortion measurement standard.

model and camera model. The distortion is measured in terms of re-projection error once all the parameters are estimated. Unfortunately this complex non-linear minimization can lead to the compensation of different errors, and reduce the precision of the estimation of the lens distortion parameters [6]. Anyway this class of methods does not provide a distortion measurement *per se*, but rather a global assessment of the camera calibration error including also other internal and external calibration parameters.

A second kind of methods directly estimates the distortion field by matching feature points on the ideal pattern to the corresponding points on a photograph of it. A continuous distortion field can be computed using interpolation techniques on discrete matching points. Several variants exist depending on the kind of pattern, matching and interpolation technique. A common assumption for these methods is that the pattern is flat. In practice, however, it is difficult to produce a very flat pattern, and the consequences of a tiny flatness flaw are considerable. For example it is reported in [7] that a flatness error of about 100 $\mu$m for a 40 centimeters broad pattern can lead to an error of about 0.3 pixels in the distortion field computation for a Canon EOS 30D camera of focal length 18 mm with the distance between the camera and the object about 30 cm. The only physical method to assess a pattern flatness at a high precision is interferometry, but it requires the pattern to be a mirror, which

is not adequate for photography. Furthermore, camera calibration requires large patterns, which are therefore flexible. Deformations of the order of 100 $\mu$m or more can be caused by temperature changes, and by a mere position change of the pattern, which deforms under its own weight.

Recently, more attention has been paid to pattern-free methods (or self-calibration methods) where the estimation of distortion is obtained without using any specific pattern. The distortion is estimated from the correspondences between two or several images in absence of any camera information. The main tool is the so-called enlarged epipolar constraint, which incorporates lens distortion into the epipolar geometry. Some iterative [8,9] or non-iterative methods [10–20] are used to estimate the distortion and correct it. All of these methods minimize the algebraic error in the estimate of the enlarged fundamental matrix, which does not give a clear geometric meaning for the distortion measurement. These methods therefore do not propose a calibrated distortion measurement.

The so called "plumb-line" methods, which correct the distortion by rectifying distorted images of 3D straight lines, date back to the 1970s (see Brown's seminal paper in 1971 [21]). Since then, this idea has been applied to many distortion models: the radial model [22–24], the FOV (Field Of View) model [25], or the rational function model [26]. These methods minimize the straightness error of the corrected lines. According to the fundamental theorem to be introduced in section 2, the plumb-line methods minimize an error directly related to the distortion, without suffering of the above mentioned drawback, namely a numerical error compensation. On the other hand, in spite of their name, plumb-line methods usually involve flat patterns with alignments on them.

Nevertheless, taken literally, these methods should use photographs of 3D straight lines. When a high precision is required, this setup becomes much easier to build than a flat pattern. The main purpose of this article is to analyze the promising properties of a basic plumb line tool, which we called "calibration harp". The calibration harp is nothing but a frame supporting tightly stretched strings. Nevertheless, the photographs of a calibration harp require a new numerical treatment to exploit them. The strings will have to be detected at high sub-pixel accuracy and their distortion converted into an invariant measurement.

Distortion measurements can be used to evaluate the distortion of a camera, but also its residual distortion after correction. Two aspects of the measurement should be clarified here. In this paper we discuss distortion measurements that apply to the camera conceived as a whole: It is impossible to tell which part the relative position and deformation of the CCD, and the lens distortion itself play in the global camera distortion. The distortion measurement is therefore not a pure optical lens distortion measurement, but the distortion measurement of the full acquisition system of camera+lens in a given state. Different lenses on different cameras can be compared only when the camera calibration matrix is known. On the other

hand, the residual error due to different correction algorithms can be compared objectively after applying an appropriate normalization on the corrected images.

This paper is organized as follows: The fundamental theorem characterizing undistorted cameras is introduced in section 2. Section 3 uncovers the simple fabrication secrets of calibration harps. The image processing algorithms needed for an automatic measurement are presented in section 4 and section 5 introduces the three most relevant measures. Section 6 gives an experimental validation, and section 7 demonstrates two applications, to the measurement of residual distortion after applying a calibration method, and to the automatization of existing manual distortion correction methods. Finally, section 8 concludes the paper.

## 2.   From Straight Lines to Straight Lines

In multiple-view geometry, the pinhole camera is the ideal model that all techniques tend to approximate at best by calibrating the real cameras. This model corresponds to the ideal geometric perspective projection. The next theorem characterizes perspective projections by the fact that they preserve alignments. The proof of the theorem can be found in [6].

**Theorem 1** *Let* $\mathbf{T}$ *be a continuous map from* $\mathcal{P}^3$ *to* $\mathcal{P}^2$ *(from 3D projective space to 2D projective plane). If there is a point* $\mathbf{C}$ *such that:*

(a) *the images of any three point belonging to a line in* $\mathcal{P}^3$ *not containing* $\mathbf{C}$*, are aligned points in* $\mathcal{P}^2$*;*

(b) *the images of any two points belonging to a line in* $\mathcal{P}^3$ *containing* $\mathbf{C}$*, are the same point in* $\mathcal{P}^2$*;*

(c) *there are at least four points belonging to a plane not containing* $\mathbf{C}$*, such that any group of three of them are non aligned, and their images are non aligned either;*

*then* $\mathbf{T}$ *is a pinhole camera with center* $\mathbf{C}$*.*

This theorem provides us with a fundamental tool to verify that a camera follows the pinhole model. Some comments about the hypotheses are pertinent. Hypothesis (a) is the main one: $\mathbf{T}$ maps lines into lines. However, this is limited to lines not passing through the camera center. Lines described by light rays entering the camera map into just one point on the image plane (when in focus), as required by hypothesis (b). Finally, hypothesis (c) is just needed to discard degenerate cases that would map the whole space $\mathcal{P}^3$ onto a single line.

Theorem 1 also provides the theoretical foundation for lens distortion measurements and justifies the use of line patterns as the more natural one. It is also the basis of the "plumb-line" distortion correction methods that recover a pinhole camera from distorted images. The theorem provides a necessary and sufficient condition. Thus, compared to the other more

indirect methods (global calibration, flat patterns), plumb-line methods seem to minimize the right error.

Nevertheless, *rectifying straight lines does not define a unique distortion correction*: two corrections can differ by any 2D homography that preserves all alignments. More concretely, assume that the real camera model is $\mathbf{P} = \mathcal{D}\mathbf{KR}[\mathbf{I} \mid -\mathbf{C}]$ with $\mathbf{C}$ the coordinate of camera optic center in a given 3D world frame, $\mathbf{R}$ the camera $3 \times 3$ orientation matrix, $\mathbf{K}$ the camera $3 \times 3$ calibration matrix and $\mathcal{D}$ the camera lens non-linear distortion. The estimated distortion can be written as $\mathcal{D}\mathbf{H}^{-1}$ with $\mathbf{H}^{-1}$ the unknown homography introduced in the distortion correction and can be different from one correction algorithm to another. By applying the inverse of the estimated distortion, the recovered pinhole camera is $\hat{\mathbf{P}} = \mathbf{HKR}[\mathbf{I} \mid -\mathbf{C}]$. The homography $\mathbf{H}$ can enlarge or reduce the straightness error, which makes the comparison of different correction algorithms unfair. This effect can be compensated by two strategies.

To arrive at a universal measurement, a first strategy that we will consider is to normalize the homography:

1. Select four points $\mathbf{P}_{i=1,...,4}$ in the distorted image in general position (not three of them aligned). For example, they can be the four corners of the distorted image.

2. Find their corresponding points $\mathbf{P}'_i$ in the corrected image, according to the correction model: $\mathbf{P}'_i = \mathbf{H}\mathcal{D}^{-1}\mathbf{P}_i$. Note that $\mathbf{H}$ is different from one correction algorithm to another.

3. Compute the normalization homography $\hat{\mathbf{H}}$ which maps $\mathbf{P}'_i$ to $\mathbf{P}_i$: $\mathbf{P}_i = \hat{\mathbf{H}}\mathbf{P}'_i$. Note that $\hat{\mathbf{H}}$ is different from one correction algorithm to another.

4. Apply the normalization homography $\hat{\mathbf{H}}$ on the corrected image.

With this normalization, the final correction model is $\hat{\mathbf{H}}\mathbf{H}\mathcal{D}^{-1}$.

A second possible strategy would be to fix specific parameters in the correction model. For example, since the zoom factor in the distortion correction is mainly determined by the order-1 parameters in the correction model, it is sufficient to set all the order-1 parameters to be 1 to obtain a unique distortion measurement. Unfortunately, this will not be possible for some non-parametric distortion correction methods. The first strategy therefore is more general.

## 3. Building a Calibration Harp

Theorem 1 suggests to photograph physically straight lines, as a calibration pattern. The obvious advantage on 2D patterns is that it is much easier to ensure a very precise physical straightness for lines than a very precise physical flatness for a physical pattern plate. The precision of the resulting measurement or correction will depend on the straightness of the

physical lines used. Yet, in the literature on plumb-line methods, there is surprisingly no detail about experimental setups: what kind of physical lines, how to ensure their straightness, how to photograph, detect, and extract them?

A common practice actually contradicts the plumb-line basic idea: line patterns are printed and pasted over a flat plate. There are many sources of imprecision in this setup: the printer quality is not perfect; the paper thickness is not perfectly uniform; the pasting process can add bubbles or a non uniform glue layer; the supporting surface is not perfectly flat either. Notwithstanding these defects, if only a pixel precision is required, this setup is quite sufficient. Nonetheless, when high sub-pixel precision is involved, the flatness errors cannot be neglected. For current camera precision, a flatness error of 100 $\mu$m (the thickness of current writing paper) for a 40 cm pattern can lead to errors in the observed image coordinates of about 0.3 pixels [7]. High precision aims at final 3D reconstructions at least as precise as this, so the base measuring tool error should be much smaller.

In contrast, it is relatively easy, as we shall now see, to build a high quality calibration pattern by tightly stretching strings on a frame, see Fig. 2. The pattern looks like the musical instrument, hence its name. The setup warrants the physical straightness of the lines. A little care is however needed in its construction to reduce the still possible sources of imperfections. The quality of the strings matters. Some strings have uneven width; twisted strings show local width oscillations. Some strings do not have a round section, and a little torsion also results in width variations that can have a long period. Rigid strings may have a remanent curvature. Finally, a (tiny) gravity effect can be avoided by using well stretched vertical lines.

In our experiments three different strings were tested: a sewing string, a smooth tennis racket string, and an opaque fishing string, see Fig. 3. Sewing strings have a braid pattern and their thickness oscillates. Tennis racket strings are rigid and require a very strong tension to become straight. Fishing strings are both smooth and flexible, and can therefore be easily tightened to be very straight. The transparent ones, however, behave like a lens, producing multiple complex edges. Opaque fishing strings end up being the best choice to build a calibration harp. Fig. 4 shows an evaluation of the obtained straightness.

To ensure the precision of the edge detection in the string images, a uniform background whose color contrasts well with the string color must be preferred. Using an opaque background is not a good idea because this requires a direct lighting and the strings project shadows on the background (Fig. 2a and 2c). The sky itself is hardly usable: a large open space is needed to avoid buildings and trees entering the camera field of view, and clouds render it inhomogeneous, see Fig. 5. The simplest solution is to place a translucent homogeneous paper or plastic sheet behind the harp and to use back illumination, preferably natural light to make it more uniform (see Fig. 2b and 2d).

The acquisition aspects are also important for producing high quality measurements: lens

(a) The harp with a uniform opaque object as background
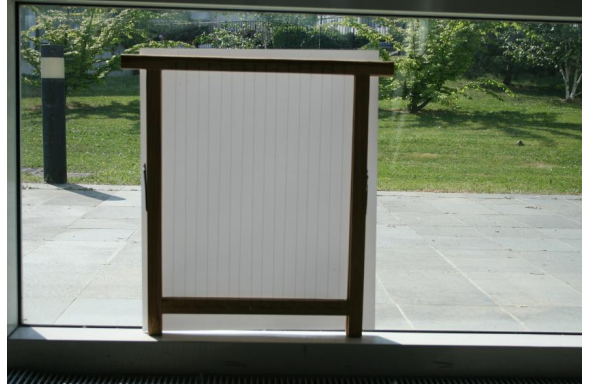


(b) The harp with a translucent paper as background



(c) A close-up of the harp with a uniform opaque object as background



(d) A close-up of the harp with a translucent paper as background

Fig. 2: The "calibration harp". Shadows can be observed in (a) and (c), while there is no shadow in (b) or (d).

blur, motion blur, aliasing, noise, must be as reduced as physically possible. To that aim a tripod and timer were used to reduce camera motions, but also to avoid out of focus strings while taking photos at different orientations. Of course, changing focus changes the distortion. Thus each distortion calibration must be done for a fixed focus, and is associated with this focus.

## 4. Straight Edges Extraction

In this section we describe the procedure to extract accurately and smooth the aligned edge points, which will be used to measure the distortion.

Devernay's algorithm [27] is the classic sub-pixel accurate edge detector. Fig. 6 shows an example. The implementation of Devernay's detector is very simple since it is derived from
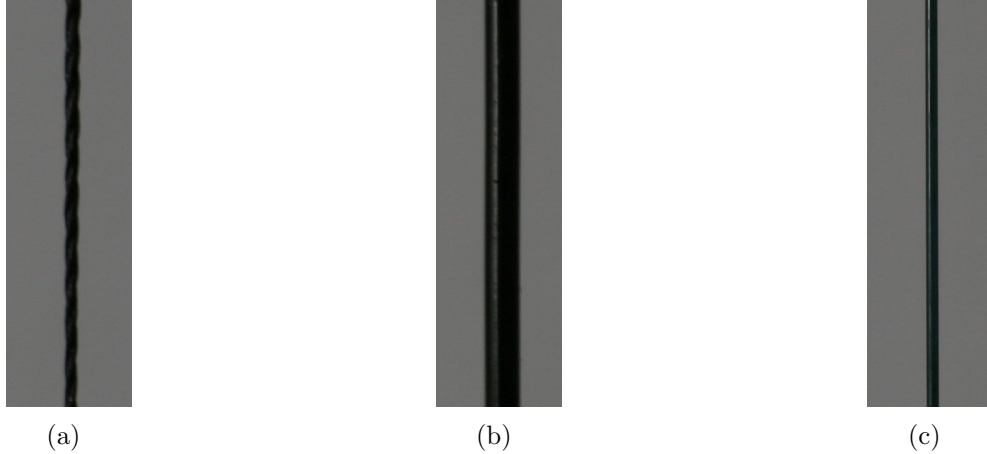
Fig. 3: Three types of strings. (a) sewing line. (b) tennis racket line. (c) opaque fishing line.

the well-known Non-Maxima Suppression method [28, 29]. On good quality images (SNR larger than 100), Devernay's detector can attain a precision of about 0.05 pixels. Some precision results are shown in section 5.

Straightness measurements require the detection of groups of edge points that belong to the same physical straight line, and the rejection of points that do not belong to any line. To this aim, line segments are detected on the image using the LSD algorithm [30, 31]. When applied to photographs of the calibration harp, the detection essentially corresponds to the strings. In case of a strong distortion, one string edge could be cut into several line segments.

LSD works by grouping connected pixels into *line support regions*, see Fig. 7. These regions are then approximated by a rectangle and validated. The *line support region* links a line segment to its support pixels. Thus, Devernay's edge points that belong to the same *line support region* can be grouped as aligned; points belonging to none are ignored.

For photos of strings, almost every pixel along each side of one string is detected as an edge point at sub-pixel precision. So there are about 1000 edge points detected for a line of length of about 1000 pixels. This large number of edge points opens the possibility to further reduce the detection and aliasing noise left by the detection through a final convolution step followed by a sub-sampling. A Gaussian blur of about $0.8 \times \sqrt{t^2 - 1}$ is needed before a $t$-subsampling to avoid aliasing [32]. We have two one-dimensional signals ($x$-coordinate and $y$-coordinate of edge points) along the length of the line. The Gaussian convolution is performed on both one-dimension signals, parameterized by the length along the edge. To facilitate the sub-sampling in the following, the edge points are resampled along the length with a uniform sampling step $d = L/N$ with $L$ the length of a line and $N$ the number of extracted edge points on the line. Assume the distance between two adjacent edge points

(a) The sewing string     (b) The tennis racket string     (c) The opaque fishing string
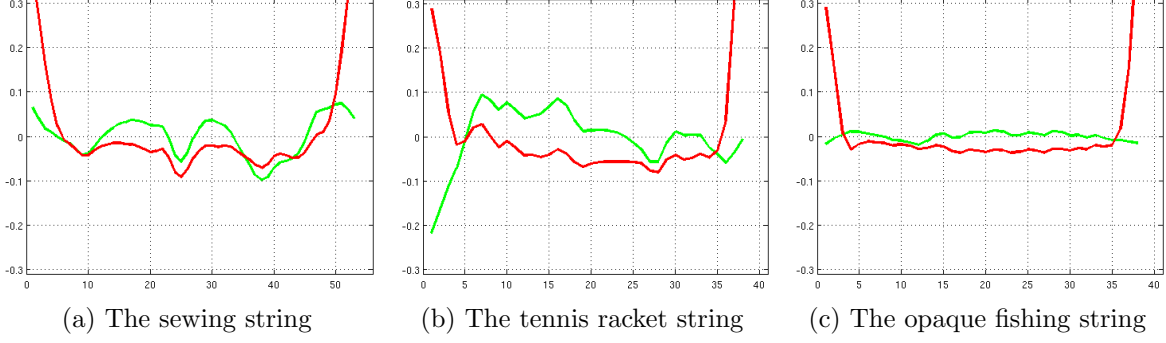
Fig. 4: The small oscillation of the corrected lines is related to the quality of the strings. The green curves show the signed distance (in pixels) from the edge points of a corrected line to its regression line. The red curves show the high frequency of the corresponding distorted line. The corrected line inherits the oscillation from the corresponding distorted line. (a) the sewing string. (b) the tennis racket string. (c) the opaque fishing line. The $x$-axis is the index of edge points. The range of the $y$-axis is from $-0.3$ pixels to $0.3$ pixels. The almost superimposing high frequency oscillation means that the high frequency of the distorted strings is not changed by the distortion correction. In such a case, the straightness error includes the high frequency of the distorted strings and does not really reflect the correction performance. So it is better to use a string which contains the smallest high frequency oscillation. Among the three types of strings, the opaque fishing string shows the smallest such oscillations. The larger oscillation of the sewing string is due to a variation of the thickness related to its twisted structure, while the tennis racket string is simply too rigid to be stretched, even though this is not apparent in Fig. 3b.

$(x_1, y_1)$ and $(x_2, y_2)$ is $l$, then the re-sampled point $(x', y')$ can be expressed as

$$
\begin{aligned}
x' &= \frac{d}{l}(x_2 - x_1) + x_1, \\
y' &= \frac{d}{l}(y_2 - y_1) + y_1,
\end{aligned}
$$

see Fig. 8. Once the line is re-sampled, the Gaussian blur $0.8 \times \sqrt{t^2 - 1}$ can be applied and is followed by a sub-sampling with factor $t$ on the $x$ and $y$ coordinates separately.

## 5. Distortion Measurements

This section examines three different natural distortion measurements that are somewhat complementary.
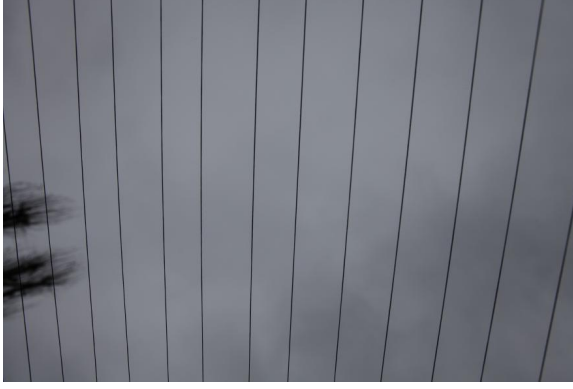
(a) Photo of the harp taken against the sky

(b) Photo of the harp taken against a translucent paper using a tripod

Fig. 5: The quality of photos depends on the harp, its background and also the stability of camera for taking photos.

### 5.A.  Root-Mean-Square Distance

According to Theorem 1, the most direct measure should be the straightness error, defined as the root-mean-square (RMS) distance from a set of distorted edge points that correspond to the same physical line, to their global linear regression line, see Fig. 9.

Given $N$ edge points $(x_1, y_1), \ldots, (x_N, y_N)$ of a distorted line, the regression line

$$\alpha x + \beta y - \gamma = 0 \tag{1}$$

is computed by

$$\alpha = \sin\theta, \quad \beta = \cos\theta, \quad \gamma = A_x \sin\theta + A_y \cos\theta,$$

where

$$A_x = \frac{1}{N}\sum_{i=1}^{N} x_i, \quad A_y = \frac{1}{N}\sum_{i=1}^{N} y_i,$$

$$V_{xx} = \frac{1}{N}\sum_{i=1}^{N}(x_i - A_x)^2, \ V_{xy} = \frac{1}{N}\sum_{i=1}^{N}(x_i - A_x)(y_i - A_y), \ V_{yy} = \frac{1}{N}\sum_{i=1}^{N}(y_i - A_y)^2,$$

$$\tan 2\theta = -\frac{2V_{xy}}{V_{xx} - V_{yy}}.$$

Since $(\alpha, \beta)$ is a unit vector, the signed distance from point $(x_i, y_i)$ to the line is given by

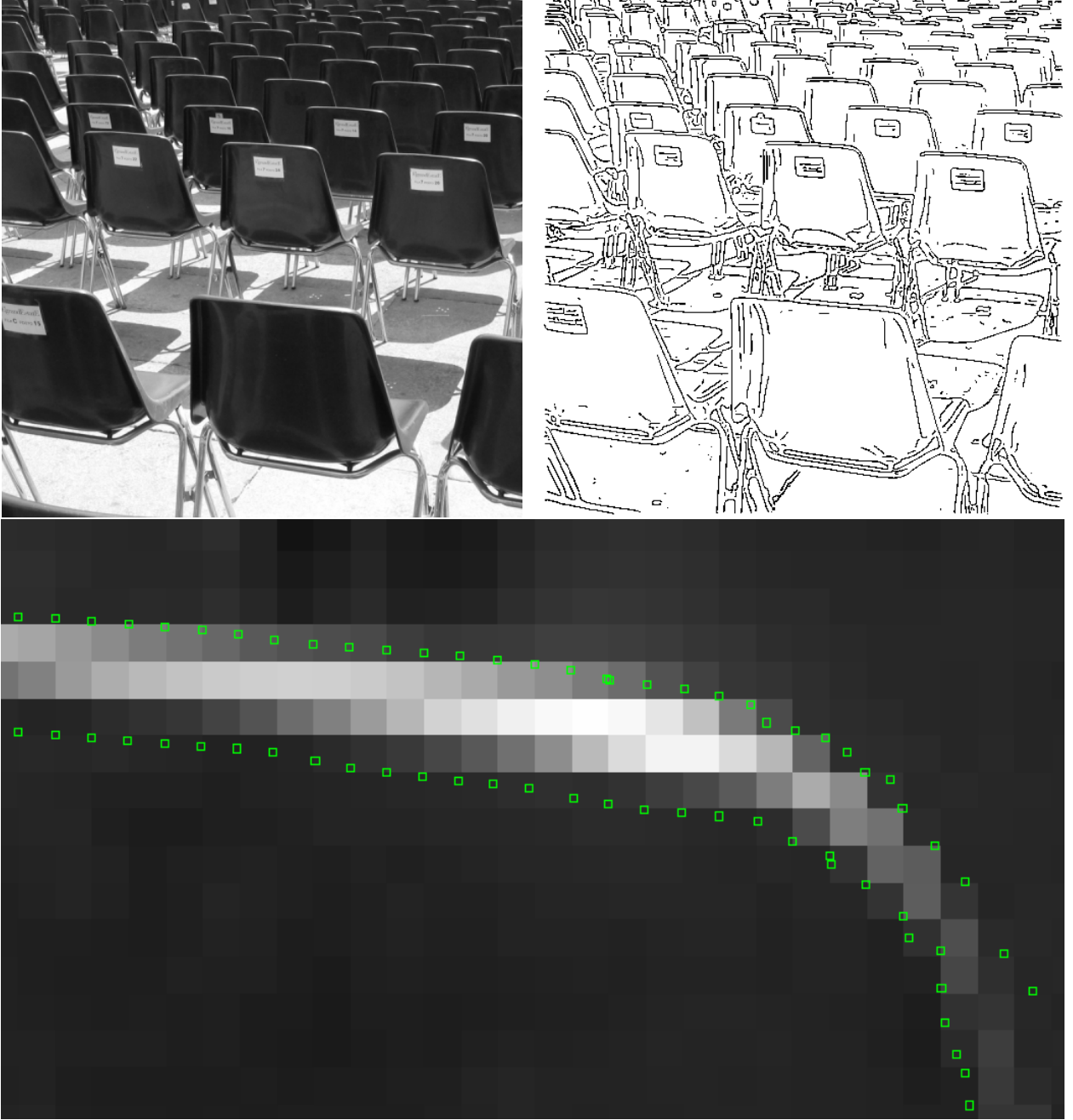$$S_i = \alpha x_i + \beta y_i - \gamma.$$

Fig. 6: Devernay sub-pixel precision edge detector. First row: the input image on the left and the resulting edge points on the right. Second row, a detail of the previous image.

Given $L$ lines, with $N_l$ points in line $l$, the total sum of squared signed distance is given by

$$S = \sum_{l=1}^{L} \sum_{i=1}^{N_l} |S_{li}|^2 = \sum_{l=1}^{L} \sum_{i=1}^{N_l} (\alpha_l x_{li} + \beta_l y_{li} - \gamma_l)^2. \tag{2}$$
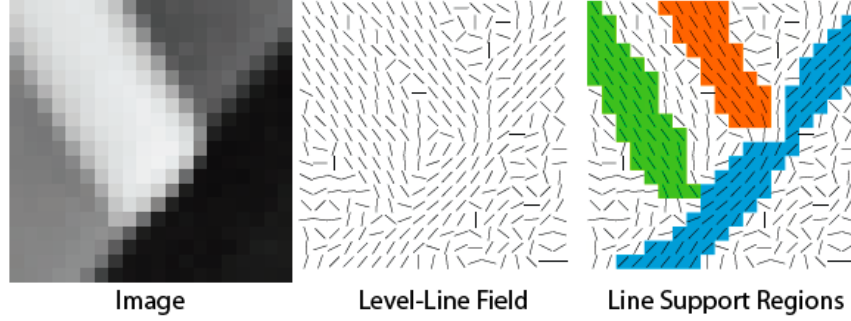
Fig. 7: The LSD algorithm computes the level-line field of the image, and then partitions the image into connected groups that share roughly the same level-line angle. They are called *line support regions*. Each such region is a candidate to line segment, and each detected line segment has a *line support region*.

Thus, the RMS straightness error is defined as

$$d = \sqrt{\frac{S}{N_T}}. \tag{3}$$

where $N_T = \sum_{l=1}^{L} N_l$ is the total number of points.

*5.B. Maximal error*

An alternative measure is the average maximal error defined by

$$d_{\max} = \sqrt{\frac{\sum_{l=1}^{L} |\max_i S_{li} - \min_i S_{li}|^2}{L}}. \tag{4}$$

In the classic camera maker practice, the maximal error is defined by

$$\max_l |\max_i S_{li} - \min_i S_{li}|,$$

which would become instable with the calibration harp, some of the strings being potentially distorted by blur or wrong detection.

 This measure is traditionally used in manual settings, for example see Fig. 1. While traditionally the measures are made relatively to the line joining the extremities of the distorted edge, see Fig. 10, here we use the signed distance to the regression line to make it more comparable to the previous measure. The use of a signed distance and the difference between the maximal and minimal value is needed to handle correctly the fact that there are values on both sides of the regression line, see Fig. 11.
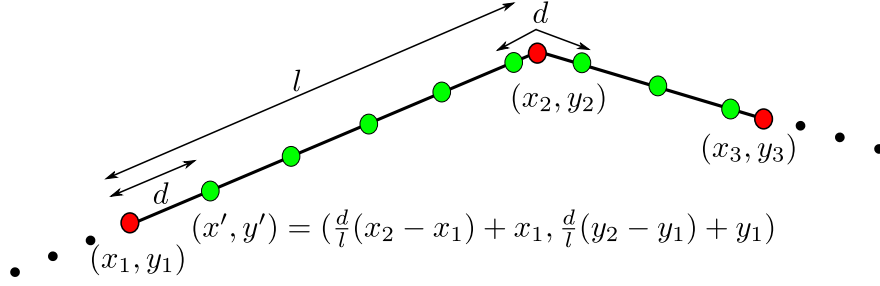
13

Fig. 8: Line re-sampling. The red points $(x_1, y_1)$, $(x_2, y_2)$, ... are the edge points extracted by Devernay's detector. They are irregularly sampled along the line. The re-sampling (in green) is made along the line with the uniform length step $d$. Linear interpolation is used to compute the re-sampled points.
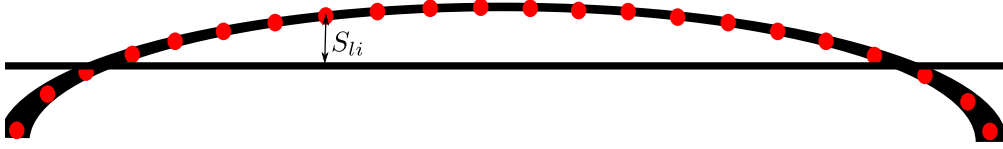


Fig. 9: The distance from a set of points to their global linear regression line.
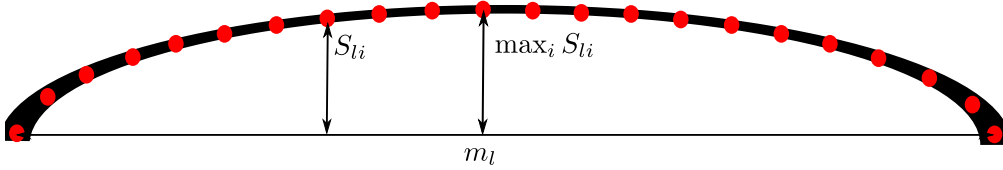


Fig. 10: Traditional distortion measure: the maximal distance to the line defined by the extremities of the edge.
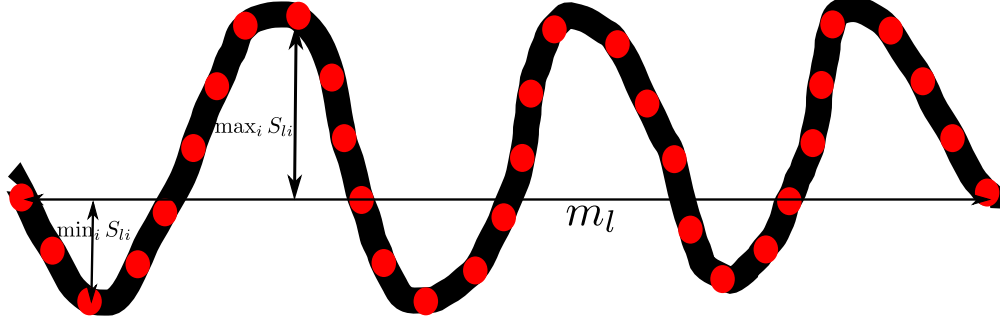
Fig. 11: The regression line crosses the distorted line; the difference between the maximal and minimal signed distance to the line measures the full width of the distorted line.

### 5.C.  Median Curvature

The previous two measures assume that the full distorted edge corresponding to a physical straight edge was well grouped. A line segment detector is designed to detect straight lines. In a distorted line it can happen that the line segment detector detects several split lines instead of one whole line, particularly when the distortion is strong. The previous measures are not robust to this effect. The last measure we consider, based on the curvature of the distorted edge, is designed to cope with it.

The curvature of a curve is a local property defined as the inverse of the radius of the osculating circle. Given three neighbor points $p_{i-1}$, $p_i$ and $p_{i+1}$, the curvature can be approximated by the following formula. (See Fig. 12.)

$$c_i = \frac{4A}{|p_{i-1} - p_i| \cdot |p_i - p_{i+1}| \cdot |p_{i+1} - p_{i-1}|} = 1/R_i \tag{5}$$

with $|p_{i-1} - p_i|$ the Euclidean distance between points $p_{i-1}$ and $p_i$ and $A$ the surface of the triangle $\Delta_{p_{i-1}p_ip_{i+1}}$. To obtain a global measure we could compute the average curvature or the average radius,

$$\bar{c} = \frac{1}{N}\sum_{i=1}^{N} c_i, \qquad \bar{R} = \frac{1}{N}\sum_{i=1}^{N} R_i = \frac{1}{N}\sum_{i=1}^{N} \frac{1}{c_i}. \tag{6}$$

But both measurements are sensitive to "outliers". The presence of one point perfectly aligned is enough to produce a large $\bar{R}$ value, while one pixel with a strong distortion, thus a large $c_i$ value, would give large $\bar{c}$ value. A more robust measurement is therefore the median of curvatures:

$$c_{\mathrm{med}} = \mathrm{median}(c_i) = 1/\mathrm{median}(R_i). \tag{7}$$

To eventually obtain a measure that is quite comparable to the previous ones, we will finally compute the maximal error that a deformation with the median curvature would produce
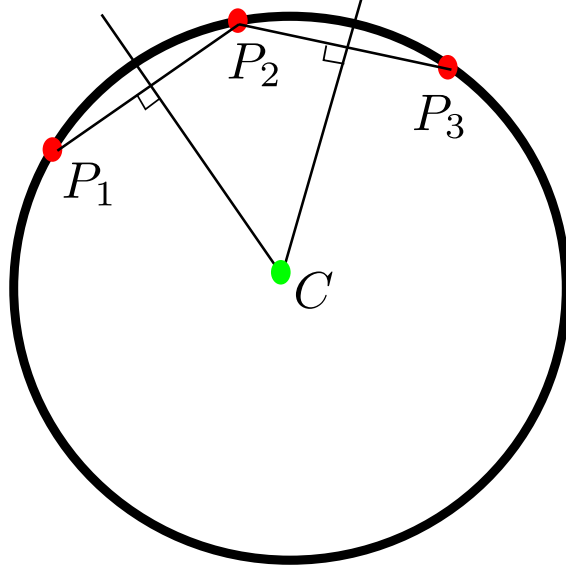
Fig. 12: Curvature computation from three points.

on the diagonal of the image, see Fig. 13:

$$d_{c_{\mathrm{med}}} = 1/c_{\mathrm{med}} - \sqrt{(1/c_{\mathrm{med}})^2 - (D/2)^2}, \tag{8}$$

where $D$ is the diagonal of the image.

## 6.   Experiments

In this section, the precision of Devernay's edge detection algorithm is first tested, by computing RMS distance of the Devernay edge points extracted from synthetic straight lines under zero noise condition. Then the proposed method will be used to measure the distortion for synthetic straight lines, arcs and sinusoidal images. Finally, real photographs of the calibration harp will be used to evaluate the residual camera distortion when this distortion has been corrected with three state-of-the-art correction methods or one popular software. Our lens distortion measurement algorithm can be tested on the online demo version available at `http://bit.ly/lens-distortion`.

### 6.A.   Devernay's Algorithm Precision

It is reported in [27] that Devernay edge points have a precision better than 0.05 pixel under zero-noise condition. To verify this precision in our implementation, synthetic images of straight edges were created, with orientation from 0° to 45° with sampling step 1°. To reduce pixelization problems, these images were created by sampling the analytic expression
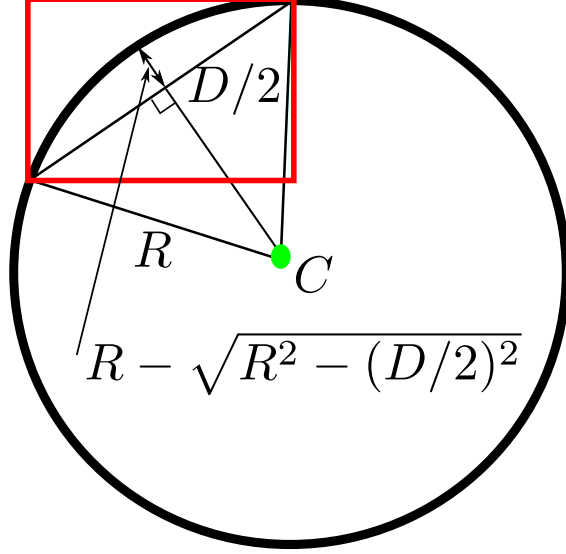
16

Fig. 13: The distortion is computed as the maximal deviation of the distorted image diagonal with the median of curvature $\mathrm{median}(R_i) = 1/\mathrm{median}(c_i)$.

of a step edge convolved by a Gaussian function of standard deviation 1. The pixel intensities computed in floating point format according to this analytic expression were rounded to one of 256 levels to emulate the analogue-to-digital conversion process of a frame grabber. Fig. 14 shows one of them. Devernay's algorithm was used to extract the edge points along the straight border in these images. In order to show the precision of Devernay's algorithm, no other post-processing is applied here, and the RMS distance $d$ in Eq. (3) was computed. Fig. 15 plots the result. The precision observed depends on the orientation, but the maximal RMS distance does not exceed 0.04 pixels (Fig. 15).

### 6.B.  Synthetic Tests

The proposed method was applied on several synthetic images. It consists of all the steps in Section 4. First a Gaussian convolution of standard deviation $0.8 \times \sqrt{t^2 - 1}$ was applied on the extracted and grouped edge points. Then the corresponding sub-sampling of factor $t$ following the Gaussian convolution was applied to compute $d$, $d_{\max}$ and $d_{c_{\mathrm{med}}}$. The only parameter to adjust here is the factor $t$, which corresponds to the assumed regularity of the lens distortion. We are only interested in realistic lens distortion, which makes a straight line globally convex or concave. Thus local edge oscillations due to noise can be harmlessly removed. In the experiments, the value of $t = 30$ pixels was chosen, which is enough to remove the local oscillation while keeping the global distortion.

Fig. 14: Synthetic image of straight lines at different orientations. Only the straight line of orientation 20° is shown here.
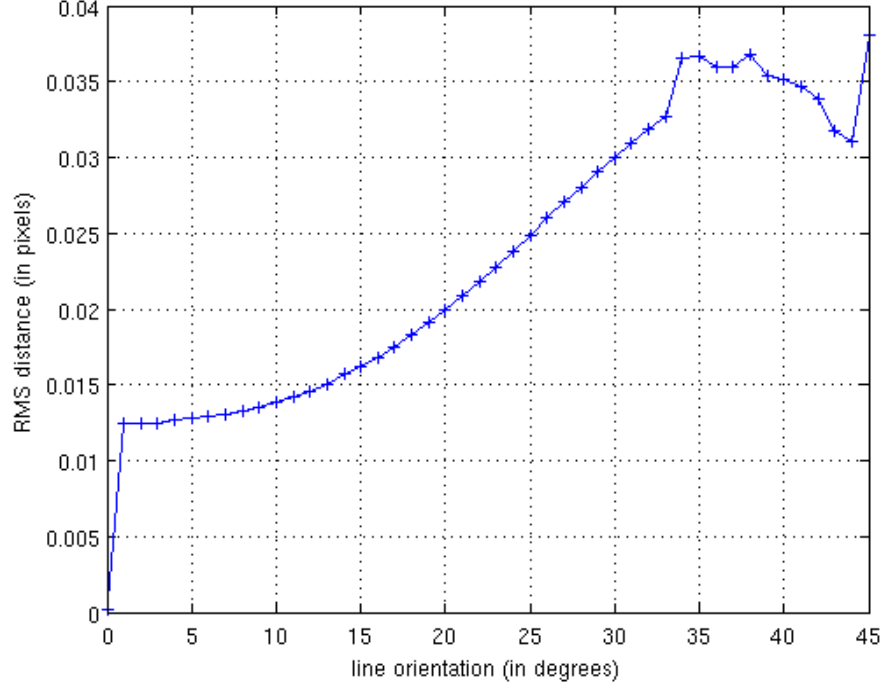
Fig. 15: RMS distance $d$ measured on the synthetic images as in Fig. 14.

### 6.B.1. Straight Lines

The first test was performed on images of size $1761 \times 1174$ containing synthetic straight lines with orientation from $0°$ to $45°$ (see one of them in Fig. 14). The measurements of $d$, $d_{\max}$ and $d_{c_{\mathrm{med}}}$ are shown in Fig. 16. This test evaluates how precise these measurements can be. Indeed, an ideal measurement should give a zero value on straight lines. The $d$ measurement gives the smallest values with respect to the other two measurements. $d_{\max}$ gives a slightly larger measurement because it gives the largest distortion with respect to the linear regression line. $d_{c_{\mathrm{med}}}$ gives the largest and the least stable measurement because it considers the distortion as the displacement on the diagonal as though the whole lines were convex, or concave.

### 6.B.2. Arcs

The second test was performed on the synthetic arcs as in Fig. 17 generated analogously as the images in Fig. 14: one arc of radius of 10000 pixels and the other of radius 100000 pixels. Both images have size $1000 \times 100$. The result in Table 1 shows a factor about 10 between the arc of radius 10000 and the arc of radius 100000. This factor is consistent with the definition of $d$, $d_{\max}$ and $d_{c_{\mathrm{med}}}$ and can be verified analytically.
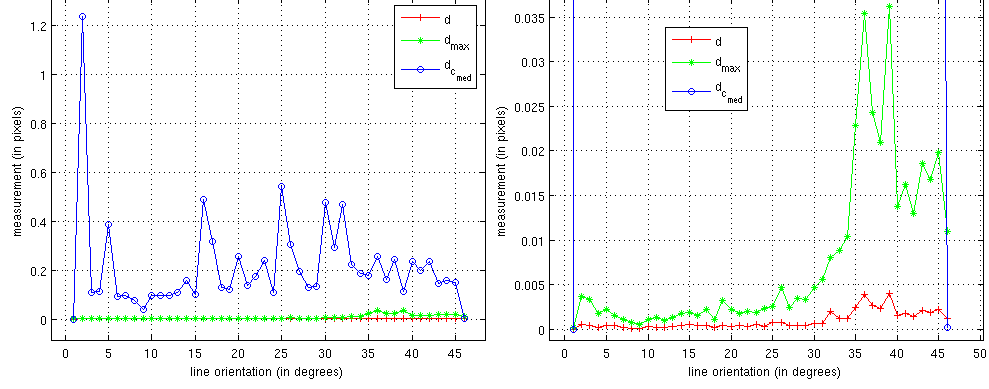
Fig. 16: RMS distance $d$, maximal distance $d_{\max}$ and curvature based measurement $d_{c_{\mathrm{med}}}$ on the synthetic straight lines shown in Fig. 14. The right image is the zoom of the left image.



(a) arc of radius 10000 pixels        (b) arc of radius 100000 pixels

Fig. 17: Arc of radius 10000 and 100000.

| radius | $d$ (pixels) | $d_{\max}$ (pixels) | $d_{c_{\mathrm{med}}}$ (pixels) |
|--------|--------------|---------------------|---------------------------------|
| 10000  | 3.59         | 11.33               | 12.59                           |
| 100000 | 0.36         | 1.09                | 1.23                            |

Table 1: RMS distance $d$, maximal distance $d_{\max}$ and curvature based measurement $d_{c_{\mathrm{med}}}$ on the synthetic arcs shown in Fig. 17.

### 6.B.3. General Distortion

Finally synthetic images of size $1761 \times 1174$, see Fig. 18, containing sinusoidal edges were generated. These edges depend on two parameters: amplitude $A$ and period $T$. In the experiments, the amplitude $A$ is fixed to 1 pixels and the period $T$ varies from 100 to 600. Table 2 shows the distortion measurements. A small period produces high frequency oscillations, that are partially reduced by the proposed method as local perturbations; the oscillations produced by a large period are measured by the method as geometric distortion. When the period is large enough all the oscillation is measured as distortion and the measures $d$ and

$d_{\max}$ approach the theoretically expected values:

$$d = \sqrt{\frac{\int_0^{T/4} A^2 \sin^2(\frac{2\pi}{T}x)dx}{T/4}} = \sqrt{\frac{A^2}{2}} \approx 0.7$$

$$d_{\max} = 2A = 2.$$

With the increase of the period, the curvature becomes smaller and so is the measurement $d_{c_{\mathrm{med}}}$. But $d_{c_{\mathrm{med}}}$ is always bigger than the corresponding $d$ and $d_{\max}$ due to the fact that $d_{c_{\mathrm{med}}}$ is computed as the displacement on the diagonal as if the whole lines were convex or concave.



(a) amplitude 1, period 100       (b) amplitude 1, period 200       (c) amplitude 1, period 300

(d) amplitude 1, period 400       (e) amplitude 1, period 500       (f) amplitude 1, period 600

Fig. 18: Sinusoidal images.

## 7. Applications

### 7.A. Measuring the residual error after distortion

As a first main application, the "calibration harp" permits to evaluate the performance of any distortion correction algorithm by measuring its residual distortion in corrected images. The procedure is as follows:

1. A series of photos of the "calibration harp" are taken at different orientations.

2. These photos are processed by a camera distortion correction algorithm.

|  | $d$ (pixels) | $d_{\max}$ (pixels) | $d_{c_{\mathrm{med}}}$ (pixels) |
|---|---|---|---|
| amplitude 1.0, period 100 | 0.23 | 0.73 | 548.41 |
| amplitude 1.0, period 200 | 0.55 | 1.66 | 288.30 |
| amplitude 1.0, period 300 | 0.64 | 2.01 | 151.84 |
| amplitude 1.0, period 400 | 0.65 | 1.96 | 88.64 |
| amplitude 1.0, period 500 | 0.68 | 1.96 | 62.26 |
| amplitude 1.0, period 600 | 0.68 | 1.96 | 53.32 |

Table 2: RMS distance $d$, maximal distance $d_{\max}$ and curvature based measurement $d_{c_{\mathrm{med}}}$ on the synthetic arcs shown in Fig. 18.

3. The corrected images are normalized by a homography as described in section 2.

4. The residual distortion is measured by the proposed method.

Three distortion correction algorithms and two software were tested. With the exception of the classic Lavest *et al.* calibration method, all the others are designed to only correct the lens distortion without estimating the other camera parameters:

- The Lavest *et al.* method [4]: probably the most advanced pattern-based global camera calibration method, which estimates and corrects for the pattern non-flatness, using a bundle adjustment technique. Various distortion parameter configurations are allowed in this method: 2 radial parameters and 2 tangential parameters for a partial distortion model; 2 radial parameters for a partial radial distortion model; 5 radial parameters for a complete radial distortion model; 5 radial parameters and 2 tangential parameters for a full distortion model.

- A non-parametric lens distortion correction method requiring a textured flat pattern [7]. The pattern is obtained by printing a textured image and pasting it on an aluminum plate, which is thick and solid.

- The DxO-Optics-Pro software: a program for professional photographers automatically correcting lens distortion (even from fisheyes), color fringing and vignetting, noise and blur. This software reads the EXIF of each image to know exactly what camera, lens and settings have been used. It therefore uses a fixed lens distortion estimation for each supported camera model.

- PTLens: Photoshop plug-in that corrects lens pincushion/barrel distortion, vignetting and chromatic aberration.

The distorted photographs to be corrected are shown in Fig. 19 and Table 3 shows the residual distortion measurements obtained by the calibration harp, after applying the corrections specified by the various methods.
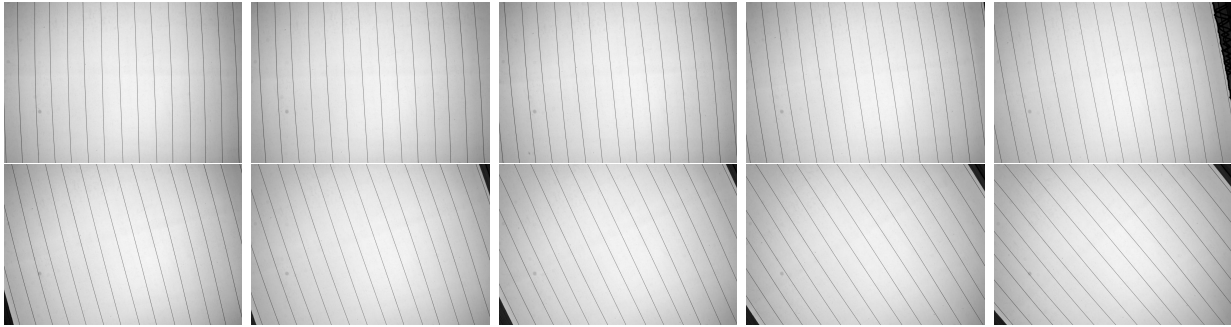


Fig. 19: The distorted photos of the "calibration harp".

| method | $d$ (pixels) | $\bar{d}_{\max}$ | $d_{c_{\mathrm{med}}}$ (pixels) |
|---|---|---|---|
| original distortion | 2.21 | 6.70 | 20.57 |
| Lavest (2 radial and 2 tangential parameters) | 0.07 | 0.30 | 5.14 |
| Lavest (2 radial parameters) | 0.07 | 0.29 | 5.08 |
| Lavest (full distortion parameters) | 0.60 | 3.00 | 6.90 |
| Lavest (full radial distortion parameters) | 0.59 | 2.90 | 6.96 |
| Textured pattern | 0.04 | 0.16 | 3.13 |
| DxO Optics Pro | 0.32 | 0.99 | 3.96 |
| PTLens | 0.46 | 1.51 | 26.49 |

Table 3: The distortion correction performance of three algorithms, measured by RMS distance $d$, maximal distance $d_{\max}$ and curvature based measurement $d_{c_{\mathrm{med}}}$.

The Lavest *et al.* method depends on the parameter configuration of the distortion model integrated in the global calibration process. Since the global calibration process only minimizes the re-projection error and does not control the distortion correction, it can happen

that the error in internal parameters compensates the error in external parameters. In consequence, the minimized re-projection error is small, but neither the estimated distortion parameters nor the other parameters are correct. In fact this is the common drawback of global camera calibration methods based on bundle adjustment. The textured pattern based method requires a perfectly flat pattern. Even though it is not very feasible to fabricate a perfectly flat pattern, a pattern made of a thick and solid aluminium plate gives a good flatness condition and thus a precise distortion correction. DxO Optics Pro includes many pre-calibrated distortion models depending on the camera type and parameters setting. But these distortion models are only calibrated on several fixed focused distances and use some interpolation techniques to obtain the distortion models focused on the other distances. Once the camera parameters are extracted from the EXIF of each image, DxO Optics Pro asks the user to manually input the focused distance before performing the correction. This makes the distortion correction result less precise; considering this, the results are surprisingly good. PTLens works in the similar manner as DxO Optics Pro except that it does not ask users to provide the focused distance information. It is not clear how PTLens recovers this information which is not available in EXIF. Probably it assumes that each focal length just focuses exactly on one distance. This coarse approximation may explain why its correction precision is not as good as DxO Optics Pro.

We also note that $d_{\max}$ and $d_{c_{\mathrm{med}}}$ are always larger than $d$. This is not surprising. Indeed, $d_{\max}$ is the biggest displacement with respect to the linear regression line of the edge points while $d_{c_{\mathrm{med}}}$ considers the distortion as the displacement on the diagonal that would result if the whole line was convex or concave. The discrepancy indicates that $d_{c_{\mathrm{med}}}$ cannot be taken alone; it may suggest a much larger distortion than what is really there. In fact, $d_{c_{\mathrm{med}}}$ makes sense before correction, when the lines are globally concave or convex, but does not make anymore sense after a distortion correction has been applied. With such corrections the lines keep some oscillation (like the synthetic test on the sinusoidal images in section 6.B.3). In short, the standards for measuring distortion of a camera are not usable after a correction has been made. This conclusion promotes $d$ (or $d_{\max}$) as the only options.

## 7.B.   *Strengthening Plumb-Line Distortion Correction Methods*

The input of plumb-line distortion correction methods are the edge points on distorted lines, which are themselves projections of 3D straight lines. It is often supposed that the edge points are already available. But in practice, it is not a trivial problem to extract aligned edge points in images. For example, the online demo [33] of Alvarez *et al.* method [22] requires the user to click manually edge points. This is on the one hand a tedious and time consuming work, and on the other hand, it may reduce the precision of edge points. The proposed method thus gives the possibility to automatize plumb-line methods. We fed four

kinds of edge points to the Alvarez *et al.* method: the first one the manually clicked edge points of a natural image (Fig. 20a), the second one the manually clicked edge points of an image of the grid pattern (Fig. 20b), the third one the the manually clicked edge points of an image of the calibration harp (Fig. 20c) and the last one the automatically extracted edge points of an image of the calibration harp (Fig. 20c), as described in section 4. Then these points were used as input to Alvarez *et al.* method to estimate the distortion model, which will be used to correct the distorted images in Fig. 19. The correction precision was again measured by the proposed method.

The results in Table 4 show that the edge points extraction part in the proposed method strengthens the plumb-line method in terms of precision and spares the long, tedious and imprecise manual point clicking task. Compared to the manual clicks with the calibration harp, the improvement in precision is moderate. This is because the Alvarez *et al.* method is applied on a very good quality photograph of the harp and the manual clicks were carefully placed on the lines across the domain of the image. The slight inaccuracy of the clicks is smoothed out by the method which applies a Gaussian convolution of the edge points along the edges. The manual clicks on the image of the grid pattern and the natural image give a precision two or three times worse than the calibration harp. For the grid pattern, the imprecision may come from the non-flatness error of the grid pattern which implies that the engraved straight lines on the pattern are not really straight. For the natural image, the imprecision comes from two aspects: one is again the non-straightness error of the lines, the other is the lack of lines at the border of the image domain, which can lead to a correction less precise at the border.

| method | time (mins) | $d$ (pixels) | $\bar{d}_{\max}$ | $d_{c_{\mathrm{med}}}$ (pixels) |
|---|---|---|---|---|
| Natural image (manually) | $\sim 5$ | 0.27 | 1.02 | 9.22 |
| Grid pattern (manually) | $\sim 25$ | 0.30 | 0.94 | 7.93 |
| Calibration harp (manually) | $\sim 30$ | 0.11 | 0.39 | 7.73 |
| Calibration harp (automatically) | $\sim 0$ | 0.08 | 0.27 | 7.39 |

Table 4: The distortion correction performance of Alvarez *et al.* method on four kinds of input edge points: manual clicks on natural image, manual clicks on grid pattern image, manual clicks on calibration harp image and automatic edge points extraction on calibration harp image and. The comparison is in terms of $d$, $d_{\max}$, $d_{c_{\mathrm{med}}}$ and the time to obtain the edge points.

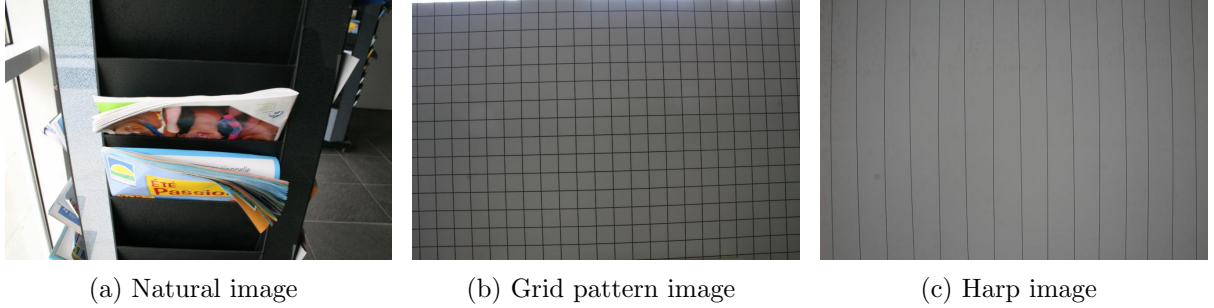(a) Natural image      (b) Grid pattern image      (c) Harp image

Fig. 20: The images used in the Lavest *et al.* method.

## 8. Conclusion

A "calibration harp" has been proposed for camera distortion measurements, along with its associated image processing chain. The precision of the method was evaluated on synthetic images and its use illustrated by measuring the residual distortion to four state-of-the-art correcting methods. In the future, we aim at combining the measurement with a high-precision distortion correction algorithm.

## References

1. C. Slama, *Manual of Photogrammetry, 4th edition* (Falls Church, American Society of Photogrammetry, Virginia, 1980).
2. R. Tsai, "A versatile camera calibration technique for high-accuracy 3d machine vision metrology using off-the-shelf tv cameras and lenses," IEEE Journal of Robotics and Automation **3**, 323–344 (1987).
3. Z. Zhang, "A flexible new technique for camera calibration," IEEE Transactions on Pattern Analysis and Machine Intelligence pp. 1330–1334 (2000).
4. J. Lavest, M. Viala, and M. Dhome, "Do we really need accurate calibration pattern to achieve a reliable camera calibration?" ECCV **1**, 158–174 (1998).
5. M. H. J. Weng, P. Cohen, "Camera calibration with distortion models and accuracy evaluation," IEEE Transactions on Pattern Analysis and Machine Intelligence **14**, 965–980 (1992).
6. Z. Tang, "Calibration de caméra à haute précision," Ph.D. thesis, ENS Cachan (2011).
7. R. Grompone von Gioi, P. Monasse, J.-M. Morel, and Z. Tang, "Towards high-precision lens distortion correction," ICIP pp. 4237–4240 (2010).
8. G. P. Stein, "Lens distortion calibration using point correspondences," CVPR pp. 602–608 (1997).

9. Z. Zhang, "On the epipolar geometry between two images with lens distortion," ICPR pp. 407–411 (1996).

10. A. Fitzgibbon, "Simultaneous linear estimation of multiple view geometry and lens distortion," CVPR **1**, 125–132 (2001).

11. B. Micusik and T. Pajdla, "Estimation of omnidirectional camera model from epipolar geometry," CVPR pp. 485–490 (2003).

12. H. Li and R. Hartley, "A non-iterative method for correcting lens distortion from nine-point correspondences," in "OmniVision," (2005).

13. S. Thirthala and M. Pollefeys, "The radial trifocal tensor: a tool for calibrating the radial distortion of wide-angle cameras," CVPR **1**, 321–328 (2005).

14. D. Claus and A. Fitzgibbon, "A rational function lens distortion model for general cameras," CVPR **1**, 213–219 (2005).

15. J. Barreto and K. Daniilidis, "Fundamental matrix for cameras with radial distortion," ICCV **1**, 625–632 (2005).

16. Z. Kukelova and T. Pajdla, "Two minimal problems for cameras with radial distortion," ICCV pp. 1–8 (2007).

17. Z. Kukelova, M. Bujnak, and T. Pajdla, "Automatic generator of minimal problem solvers," ECCV pp. 302–315 (2008).

18. M. Byrod, Z. Kukelova, K. Josephson, T. Pajdla, and K. Astrom, "Fast and robust numerical solutions to minimal problems for cameras with radial distortion," CVPR pp. 1–8 (2008).

19. Z. Kukelova and T. Pajdla, "A minimal solution to the autocalibration of radial distortion," CVPR pp. 1–7 (2007).

20. K. Josephson and M. Byrod, "Pose estimation with radial distortion and unknown focal length," CVPR pp. 2419–2426 (2009).

21. D. Brown, "Close-range camera calibration," Photogrammetric Engieering **37**, 855–866 (1971).

22. L. Alvarez, L. Gomez, and J. Rafael Sendra, "An algebraic approach to lens distortion by line rectification," Journal of Mathematical Imaging and Vision **35(1)**, 36–50 (2009).

23. B. Prescott and G. McLean, "Line-based correction of radial lens distortion," Graphical Models and Image Processing **59**, 39–47 (1997).

24. T. Pajdla, T. Werner, and V. Hlavac, "Correcting radial lens distortion without knowledge of 3-d structure," Research Report, Czech Technical University (1997).

25. F. Devernay and O. Faugeras, "Straight lines have to be straight," Machine Vision and Applications **13**, 14–24 (2001).

26. D. Claus and A. Fitzgibbon, "A plumbline constraint for the rational function lens distortion model," BMVC pp. 99–108 (2005).

27. F. Devernay, "A non-maxima suppression method for edge detection with sub-pixel accuracy," Tech. Rep. 2724, INRIA rapport de recherche (1995).

28. J. Canny, "A computational approach to edge detection," IEEE Transactions on Pattern Analysis and Machine Intelligence **8**, 679–698 (1986).

29. R. Deriche, "Using Canny's criteria to derive a recursively implemented optimal edge detector," International Journal of Computer Vision **1**, 167–187 (1987).

30. R. Grompone von Gioi, J. Jakubowicz, J. Morel, and G. Randall, "LSD: A fast Line Segment Detector with a false detection control," IEEE Transactions on Pattern Analysis and Machine Intelligence **32**, 722–732 (2010).

31. R. Grompone von Gioi, J. Jakubowicz, J. Morel, and G. Randall, "LSD: a Line Segment Detector," Image Processing On Line (2012).

32. J. Morel and G.Yu, "On the consistency of the sift method," Preprint, CMLA, ENS-Cachan (2009).

33. L. G. Luis Alvarez and J. R. Sendra, "Algebraic Lens Distortion Model Estimation," Image Processing On Line (2010).